An essential resource for scientists designing new energy materials for the vast landscape of solar energy conversion as well as materials processing and characterization

Based on the new and fundamental research on novel energy materials with tailor-made photonic properties, the role of materials engineering has been to provide much needed support in the development of photovoltaic devices. *Advanced Energy Materials* offers a unique, state-of-the-art look at the new world of novel energy materials science, shedding light on the subject's vast multi-disciplinary approach.

The book focuses particularly on photovoltaics, efficient light sources, fuel cells, energy-saving technologies, energy storage technologies, nanostructured materials as well as innovating materials and techniques for future nanoscale electronics. Pathways to future development are also discussed.

Critical, cutting-edge subjects are addressed, including:

- Non-imaging focusing heliostat; state-of-the-art of nanostructures
- Metal oxide semiconductors and their nanocomposites
- Superionic solids; polymer nanocomposites; solid electrolytes; advanced electronics
- Electronic and optical properties of lead sulfide
- High-electron mobility transistors and light-emitting diodes
- Anti-ferroelectric liquid crystals; PEEK membrane for fuel cells
- Advanced phosphors for energy-efficient lighting
- Molecular computation photovoltaics and photocatalysts
- Photovoltaic device technology and non-conventional energy applications

Readership
The book is written for a large and broad readership including researchers and university graduate students from diverse backgrounds such as chemistry, materials science, physics, and engineering working in the fields of nanotechnology, photovoltaic device technology, and non-conventional energy.

Ashutosh Tiwari is an Associate Professor at the Biosensors and Bioelectronics Centre, Linköping University, Sweden; Editor-in-Chief, *Advanced Materials Letters*; Secretary General, International Association of Advanced Materials; a materials chemist and also a docent in applied physics at Linköping University, Sweden. He has published more than 350 articles, patents, and conference proceedings in the field of materials science and technology and has edited/authored more than fifteen books on the advanced state-of-the-art of materials science. He is a founding member of the Advanced Materials World Congress and the Indian Materials Congress.

Sergiy Valyukh is an Associate Professor at the Laboratory of Applied Optics, Department of Physics, Chemistry and Biology (IFM), Linköping University, Sweden. He obtained his PhD from the Taras Shevchenko National University of Kyiv in the Ukraine. In 2003, Dr. Valyukh was invited by the Swedish LCD Center and Dalarna University to conduct research in the field of applied physics of liquid crystals. In 2008–2009, he developed several new electrooptical devices for companies producing displays, based on liquid crystals, and he was nominated by the Swedish Innovation Foundation ALMI in the category "New Developer in Dalarna Business 2009." In 2012, he became a docent in applied optics at Linköping University.

Cover designed by Russell Richardson
Cover figures courtesy of Suresh Sagadevan

Also available as an e-book

Visit us at wiley.com

WILEY

www.scrivenerpublishing.com

ISBN 978-1-118-68629-4
90000
9 781118 686294

Tiwari
Valyukh

ADVANCED ENERGY MATERIALS

WILEY

Advance Materials Series

ADVANCED ENERGY MATERIALS

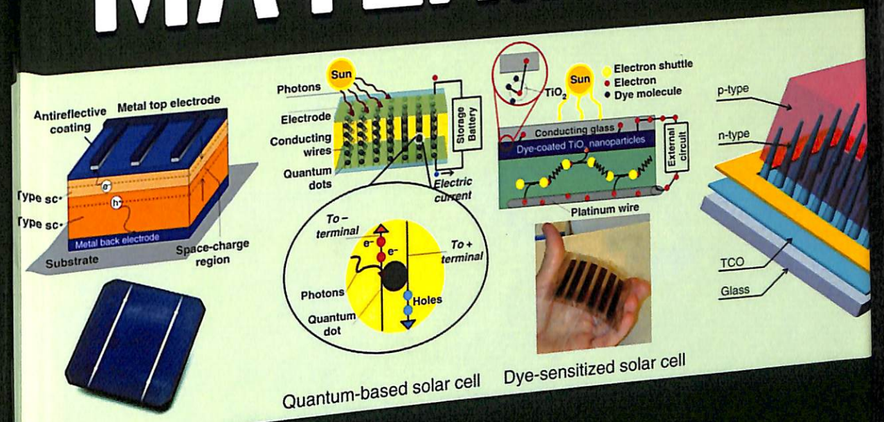

Edited By
Ashutosh Tiwari and Sergiy Valyukh

Scrivener Publishing

WILEY

An essential resource for scientists designing new energy materials for the vast landscape of solar energy conversion as well as materials processing and characterization

Based on the new and fundamental research on novel energy materials with tailor-made photonic properties, the role of materials engineering has been to provide much needed support in the development of photovoltaic devices. *Advanced Energy Materials* offers a unique, state-of-the-art look at the new world of novel energy materials science, shedding light on the subject's vast multi-disciplinary approach.

The book focuses particularly on photovoltaics, efficient light sources, fuel cells, energy-saving technologies, energy storage technologies, nanostructured materials as well as innovating materials and techniques for future nanoscale electronics. Pathways to future development are also discussed.

Critical, cutting-edge subjects are addressed, including:

- Non-imaging focusing heliostat; state-of-the-art of nanostructures
- Metal oxide semiconductors and their nanocomposites
- Superionic solids; polymer nanocomposites; solid electrolytes; advanced electronics
- Electronic and optical properties of lead sulfide
- High-electron mobility transistors and light-emitting diodes
- Anti-ferroelectric liquid crystals; PEEK membrane for fuel cells
- Advanced phosphors for energy-efficient lighting
- Molecular computation photovoltaics and photocatalysts
- Photovoltaic device technology and non-conventional energy applications

Readership

The book is written for a large and broad readership including researchers and university graduate students from diverse backgrounds such as chemistry, materials science, physics, and engineering working in the fields of nanotechnology, photovoltaic device technology, and non-conventional energy.

Ashutosh Tiwari is an Associate Professor at the Biosensors and Bioelectronics Centre, Linköping University, Sweden; Editor-in-Chief, *Advanced Materials Letters*; Secretary General, International Association of Advanced Materials; a materials chemist and also a docent in applied physics at Linköping University, Sweden. He has published more than 350 articles, patents, and conference proceedings in the field of materials science and technology and has edited/authored more than fifteen books on the advanced state-of-the-art of materials science. He is a founding member of the Advanced Materials World Congress and the Indian Materials Congress.

Sergiy Valyukh is an Associate Professor at the Laboratory of Applied Optics, Department of Physics, Chemistry and Biology (IFM), Linköping University, Sweden. He obtained his PhD from the Taras Shevchenko National University of Kyiv in the Ukraine. In 2003, Dr. Valyukh was invited by the Swedish LCD Center and Dalarna University to conduct research in the field of applied physics of liquid crystals. In 2008–2009, he developed several new electrooptical devices for companies producing displays, based on liquid crystals, and he was nominated by the Swedish Innovation Foundation ALMI in the category "New Developer in Dalarna Business 2009." In 2012, he became a docent in applied optics at Linköping University.

Cover designed by Russell Richardson
Cover figures courtesy of Suresh Sagadevan

Also available as an e-book

Visit us at wiley.com

WILEY | www.scrivenerpublishing.com

ISBN 978-1-118-68629-4

Tiwari
Valyukh

ADVANCED ENERGY MATERIALS

WILEY

Advance Materials Series

ADVANCED ENERGY MATERIALS

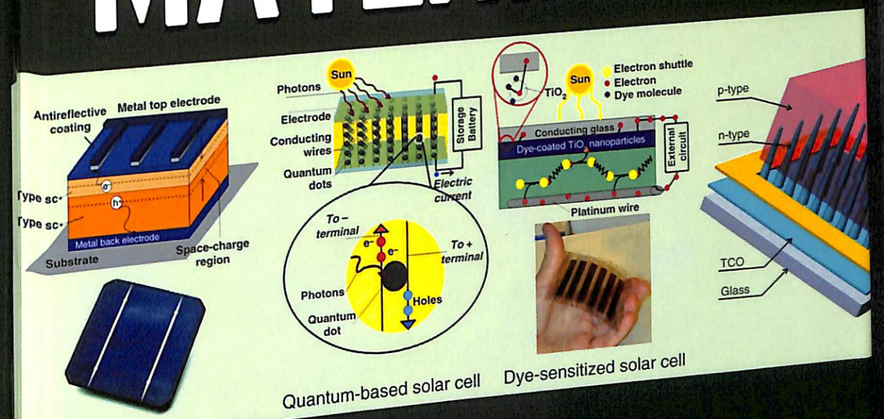

Edited By
Ashutosh Tiwari and Sergiy Valyukh

Scrivener Publishing

WILEY

Scrivener Publishing
100 Cummings Center, Suite 541J
Beverly, MA 01915-6106

Advance Materials Series

The Advance Materials Series provides recent advancements of the fascinating field of advanced materials science and technology, particularly in the area of structure, synthesis and processing, characterization, advanced-state properties, and applications. The volumes will cover theoretical and experimental approaches of molecular device materials, biomimetic materials, hybrid-type composite materials, functionalized polymers, superamolecular systems, information- and energy-transfer materials, biobased and biodegradable or environmental friendly materials. Each volume will be devoted to one broad subject and the multidisciplinary aspects will be drawn out in full.

Series Editor: Dr. Ashutosh Tiwari
Biosensors and Bioelectronics Centre
Linkoping University
SE-581 83 Linkoping
Sweden
E-mail: ashutosh.tiwari@liu.se
Managing Editors: Swapneel Despande, Sudheesh K. Shukla and Yashpal Sharma

Publishers at Scrivener
Martin Scrivener(martin@scrivenerpublishing.com)
Phillip Carmical (pcarmical@scrivenerpublishing.com)

Advanced Energy Materials

Edited by

Ashutosh Tiwari and Sergiy Valyukh

WILEY

Copyright © 2014 by Scrivener Publishing LLC. All rights reserved

Co-published by John Wiley & Sons, Inc. Hoboken, New Jersey, and Scrivener Publishing LLC, Salem, Massachusetts.
Published simultaneously in Canada.

No part of this publication may be reproduced, stored in a retrieval system, or transmitted in any form or by any means, electronic, mechanical, photocopying, recording, scanning, or otherwise, except as permitted under Section 107 or 108 of the 1976 United States Copyright Act, without either the prior written permission of the Publisher, or authorization through payment of the appropriate per-copy fee to the Copyright Clearance Center, Inc., 222 Rosewood Drive, Danvers, MA 01923, (978) 750-8400, fax (978) 750-4470, or on the web at www.copyright.com. Requests to the Publisher for permission should be addressed to the Permissions Department, John Wiley & Sons, Inc., 111 River Street, Hoboken, NJ 07030, (201) 748-6011, fax (201) 748-6008, or online at http://www.wiley.com/go/permission.

Limit of Liability/Disclaimer of Warranty: While the publisher and author have used their best efforts in preparing this book, they make no representations or warranties with respect to the accuracy or completeness of the contents of this book and specifically disclaim any implied warranties of merchantability or fitness for a particular purpose. No warranty may be created or extended by sales representatives or written sales materials. The advice and strategies contained herein may not be suitable for your situation. You should consult with a professional where appropriate. Neither the publisher nor author shall be liable for any loss of profit or any other commercial damages, including but not limited to special, incidental, consequential, or other damages.

For general information on our other products and services or for technical support, please contact our Customer Care Department within the United States at (800) 762-2974, outside the United States at (317) 572-3993 or fax (317) 572-4002.

Wiley also publishes its books in a variety of electronic formats. Some content that appears in print may not be available in electronic formats. For more information about Wiley products, visit our web site at www.wiley.com.

For more information about Scrivener products please visit www.scrivenerpublishing.com.

Cover design by Russell Richardson

Library of Congress Cataloging-in-Publication Data:

ISBN 978-1-118-68629-4

Printed in the United States of America

10 9 8 7 6 5 4 3 2 1

Contents

Preface

Energy plays a critical role in the developmental progression of an emerging society. A high standard of living and an increasing world population require more and more amounts of energy. At the same time, the standard energy sources based on fossil fuels are limited and pollute the environment, leading to climate change on a global scale. In order to avoid an energy crisis, the research efforts of many scientific centers around the globe are being directed towards searching for new solutions and improving those already existing in the energy sector. In parallel with the growth rate of renewable energy, essential attention is being paid to the development of advanced methods and materials for effective utilization of energy resources. Technological advantages will help to overcome energy-related difficulties. Among the main criteria for the viability of new energetic techniques are efficiency, cost, usability and environmental influence.

This book summarizes the current status of know-how in the fields of advanced materials for energy-associated applications, in particular, photovoltaics, efficient light sources, fuel cells, energy saving technologies, nanostructured materials, etc. Tendencies for future development are also discussed. A good understanding of the excited state reactivity of photoactive materials would help to prepare new materials and molecules capable of absorbing light over a given wavelength range for use in driving electron transfer. There has been scientifically and technologically well-equipped materials science exploration into the possibility of developing and optimizing charge separation in light-harvesting architectures. However, it has yet to bear fruit due to the difficulty of transporting electrons and holes to corresponding electrodes. Modeling charge mobility in semiconductors is complicated due to the presence of bulk heterogeneity in the structure. The understanding of

the interface between the metal electrode and the active materials, where charge collection takes place, is even more intriguing.

The design and fabrication of molecular-based information processing devices on conducting substrates have been key areas of research in materials science. One particularly attractive application in this area is the conversion of solar energy into fuel, which is currently being proposed as a cheaper alternative for energy conversion. Energy storage technologies are dealt with in some chapters. High energy density capacitors are of particular significance, for example, in defense-related applications, where tasks in remote areas without traditional energy resources demand novel approaches to energy storage. Polymer nanocomposites offer attractive, low-cost potential storage systems for high-energy density capacitors. Their tailored characteristics offer unique combinations of properties which are expected to play a vital role in the development of new technologies for energy storage applications.

Other chapters consider the aspects of solar energy. Rapid progress in photovoltaic science and technology during the last decades is a reason that solar cells came out of the laboratories and are becoming a part of our everyday life. And this is only the beginning of the era of solar energy. The number of reports about new approaches in this field is increasing dramatically. Among the reported topics are nanostructure compositions, transparent conductors, inclusion of metal oxide as well as metal-based thin films, light-trapping schemes that enable increased conversation efficiency, various concentrators and solar tracking systems, etc. Chapters two through ten are devoted to consideration of innovative materials and techniques for future nanoscale electronics. Two allotropic forms of carbon, carbon nanotubes and graphene, are able to replace conducting channels and silicon in elements of integrated circuits, thereby opening a new era of carbon-based electronics which will lead to denser, faster and more power-efficient circuitry. A possible attractive alternative to the semiconductor components in digital processing devices is chip-based molecular logic gates—molecules possessing the property to perform logical operations where a chemical or physical binary input to the molecules causes a binary output. Surface-confined materials showing switching behavior along with changes in physical properties (i.e., optical, orientation, magnetism) make it possible to create integrated complex circuits for massive networking systems. Significant attention is being paid to the development of fuel cells—devices that convert chemical

energy from a fuel into electricity through a chemical reaction with oxygen or another oxidizing agent. Because there is no combustion in the energy conversion process, fuel cells are efficient and environmentally friendly. The fuel cell market is also growing at a fast pace, and according to Pike Research, the stationary fuel cell market is predicted to reach 50 GW by 2020. There is a chapter describing the problems related to energy efficient lighting, In particular, vanadate phosphors are considered—luminescent materials that have excellent thermal and chemical stability. Phosphor layers provide most of the light produced by fluorescent lamps, and are also used to improve the balance of light produced by metal halide lamps.

Also discussed in the book is the role of materials engineering in providing much needed support in the development of photovoltaic devices with new and fundamental research on novel energy materials with tailor-made photonic properties. This book is written for a large readership, including university students and researchers from diverse backgrounds such as chemistry, materials science, physics, pharmacy, medical science and engineering. It can be used not only as a textbook for both undergraduate and graduate students, but also as a review and reference book for researchers in materials science, nanotechnology, photovoltaic device technology and non-conventional energy. We hope the chapters herein will provide readers with valuable insight into the state-of-the-art of advanced and functional materials and cutting-edge energy technologies. The main credit for this book must go to the authors of the chapters who have summarized information in the field of advanced energy-related materials.

Editors
Ashutosh Tiwari, Docent, PhD
Sergiy Valyukh, Docent, PhD

6

Solid Electrolytes: Principles and Applications

S.W. Anwane

Department of Physics, Shri Shivaji Science College, Congress Nagar, Nagpur, India

Abstract

Solid electrolytes (SEs), commonly known as super ionic conductors (SICs) or fast ionic conductors (FICs), form a special class of ionic solids that offer high ionic conductivity, i.e., in the range of 0.01–0.1 S/cm. Japanese researcher Takehiko Takahashi was one of the pioneers in the field who pointed out the ionic conductivity of solid material $Ag_6I_4WO_4$ comparable to liquid electrolytes. This compound has a silver ion conductivity of 0.047 S/cm at 25°C and activation energy of 3.6 kcal/mole for conduction between 20 and 293°C. Since then, this area has gained tremendous attention due to the fascinating possibility of a wide range of applications that include electrochemical devices like solid-state batteries, pacemakers, solid-state gas sensors, etc.

The mobility of cation in the lattice of solids contributing to high conductivity depends upon various parameters that include: number of mobile cations, its size, mobility, lattice structure and defects, available vacancy positions, conduction mechanism, etc. Depending upon various factors, these materials have been classified in numerous ways. However, the most general approach involves classification as (a) crystalline, (b) non-crystalline and (c) composites. The majority of crystalline SEs possess typical crystal structure in which a number of symmetrical vacant sites are available for mobile cations which need to be energetically equivalent for promoting migration of ions. Glassy and polymer SEs form extremely disordered type non-crystalline materials. The ionic conductors containing dispersed second phase particles commonly form a class known as composites.

**Corresponding author:* swanwane2000@yahoo.com

Ashutosh Tiwari and Sergiy Valyukh (eds.) Advanced Energy Materials, (259–294)
2014 © Scrivener Publishing LLC

Various criteria which promote high ionic mobility, and in turn high ionic conductivity, have been thoroughly studied. Different conduction models which have been studied so far include Independent particle model, single particle hopping model, continuous diffusion, free ion, cooperative motion, lattice-gas model, fractals and Debye Huckel model, etc.

A vast growth in the users of electrochemical devices which employ SEs has generated a need of miniaturization, corrosion free reversible reactions, weight effectiveness, etc. Though this has been potentially conquered in the past few years, the hunt for an apt material is endless.

Keywords: Solid electrolytes, super ionic conductors, fast ionic conductors, solid-state batteries, electrochemical gas sensor

6.1 Introduction

In solids the atoms are rigidly fixed in their position except for a little vibration. The properties of solids depend upon their structure. In 1912 Laue first demonstrated X-ray diffraction of crystal. There are forces which hold these atoms at fixed positions. There must be several attractive forces counterbalanced by repulsive forces. Every atom consists of a nucleus that is surrounded by electron cloud (shells). A shell is more stable if closed. If not closed, it gains or loses electron/s to obtain a number that makes it closed or stable. According to bonding type, the types of solids can be specified as: ionic bond, covalent bond, metallic bond, hydrogen bond, van der Waals/molecular bond.

Atoms are bound together as electron when one atom is transferred to another, enabling both the status of "closed-shell" electronic structure. The formation of a pair of ions by transfer of electron from one atom to another creates Coulombian attractive force counterbalanced by repulsive force and gives a fixed distance to the ionic bond.

The considered formation of MX bond is:

$$M \rightarrow M^{+} + e^{-} \tag{6.1a}$$

$$X + e^{-} \rightarrow X^{-} \tag{6.1b}$$

In the above process a certain energy is required. The process of formation of cations (M^{+}) is endothermic since some work has to be

done against attraction between nuclei and electron. This is termed as ionization energy (I_M). When an electron is added to X, energy is released in anion formation. But for addition of more than one electron the process becomes endothermic due to repulsive interaction by X^{-}. The isolated ions M^{+} and X^{-} approaching each other from infinity acquire Coulombic attraction counterbalanced by repulsive force at the bond length. The potential energy due to Coulombic attraction between two ions is given by:

$$\varnothing_{coulomb} = -\frac{Z_1 Z_2 e^2}{r} \tag{6.2}$$

The short range repulsive energy is:

$$\varnothing_{rep} = -be^{-r/\rho} \tag{6.3}$$

$$\varnothing_{tot} = \varnothing_{rep} + \varnothing_{coulomb} \tag{6.4}$$

$$\varnothing_{tot} = -\frac{Z_1 Z_2 e^2}{r} - be^{-r/\rho} \tag{6.5}$$

At equilibrium separation $r = r_0$, it is minimum and, hence,

$$\frac{d}{dr}\varnothing_{tot} = 0 \tag{6.6}$$

Thus at equilibrium separation ($r = r_0$),

$$\varnothing_0 = -\frac{Z_1 Z_2 e^2}{r_0}\left(1 - \rho / r_0\right) \tag{6.7}$$

Therefore the net energy involved in formation of stable ionic bonds per g-mol would be:

$$\Delta H = I_M - E_X - N_0 \frac{Z_1 Z_2 e^2}{r_0}\left(1 - \frac{\rho}{r_0}\right) \tag{6.8}$$

where N_0 is Avogadro's number.

Energy evolved (negative value of ΔH) favors ionic bond formation.

{e.g., ΔH = -80*kcal/mole* for NaCl, ΔH = -88*kcal/mole* for MgO}

6.2 Ionic Solids

In solid-state ionics, fast ion conductors (FICs), also known as solid electrolytes (SEs) and super-ionic conductors (SICs) [1], are materials that act as solid-state ion conductors and are used primarily in solid oxide fuel cells, solid-state batteries, electrochemical gas sensors, etc. The solid electrolytes conduct due to the movement of ions through voids, or empty crystallographic positions, in their crystal lattice structure. The most commonly used solid electrolyte is yttria-stabilized zirconia (YSZ). One component of the structure, the cation or anion, is essentially free to move throughout the structure, acting as a charge carrier.

Conduction through the space-charge layer of ionic crystals is one of the fascinating phenomena that gives rise to high ionic conductivity in solids. Such conduction was first predicted by Kurt Lehovec [2]. As the space-charge layer has nanometer thickness, the effect is directly related to nano-ionics. Lehovec's effect is used as a basis for developing nanomaterials for portable lithium batteries and fuel cells.

Fast ion conductors are intermediate in nature between crystalline solids which possess a regular structure with immobile ions, and liquid electrolytes which have no regular structure and fully mobile ions. Solid electrolytes find use in all solid state supercapacitors, batteries and fuel cells, and in various kinds of electrochemical sensors.

6.2.1 Bonds in Ionic Solids

The case of finding repulsive energy using the Coulombian equation for an isolated atom is quite easy, say 88 *kcal/mole* for MgO [3]. However, in crystal it may be calculated by summing up individual effects. If the charge on i^{th} and j^{th} ion are e_i and e_j, respectively, which are separated by distance r_{ij}, the Coulombian interaction at i can be given as:

$$\left(\varnothing_i\right)_{crystal} = -e_i \sum_{j, j\neq i}^{n} \frac{e_j}{r_{ij}} \tag{6.9a}$$

$$\left(\varnothing_i\right)_{crystal} = -Ne_i \sum_{j, j\neq i}^{n} \frac{e_j}{r_{ij}} \tag{6.9b}$$

By considering only the nearest neighboring interaction and approximations, we can write:

$$\left(\varnothing_{coul}\right)_{crystal} = N(nbe^{-\frac{R}{\rho}} - ae^2 / R) \tag{6.10a}$$

A typical plot of as a function of $\varnothing_{coul}$ has been presented for arbitrary values of constants as shown in Figure 6.1. Following syntax in Maple 14 can generate it with a choice of associated constants, while Table 6.1 presents few worked out examples of Madelung [3,4] constant.

$$plots_{implicitplot}\left(\Phi = 3.000000000e^{-R} - \frac{0.7500000000}{R}, R = -5..5, \Phi = -5..5, labels = [R, \Phi]\right) \tag{6.10b}$$

where, $e_i = e_1 = e, r_{ij} = p_{ij}R = R, Madelung\ constant\ a = \sum_j \frac{(\pm)}{p_{ij}}$

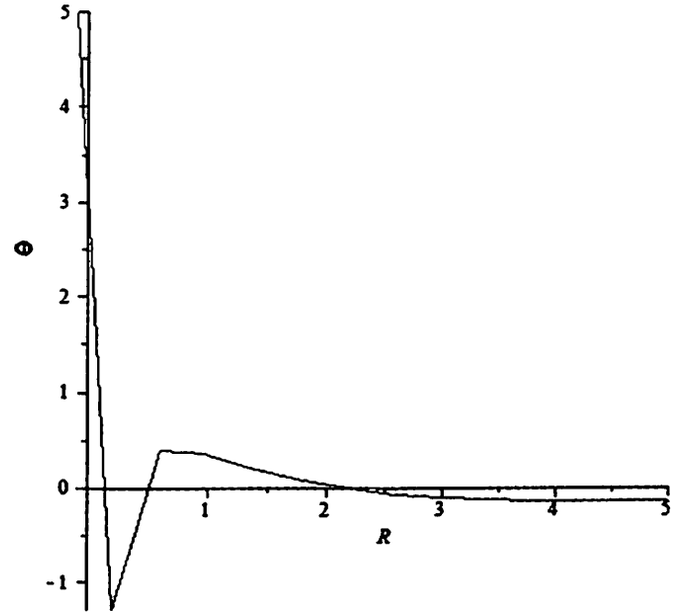

Figure 6.1 A typical potential pot for $\left(\varnothing_{coul}\right)_{crystal} = N(nbe^{-\frac{R}{\rho}} - ae^2 / R)$

Table 6.1 Lattice and Madelung Constant [4].

Sr No	Lattice	Madelung Constant (α)
1	ZnS	1.6381
2	$NaCl$	1.7476
3	TiO_2	4.816
4	CaF_2	5.039
5	Al_2O_3	25.031

The plus sign is taken for like charges and minus for unlike charges.

6.2.2 Structure of Ionic Solids

In 1974 Adams [5] explained most of what is known as ionic structure.

- Anions may be treated as charged, incompressible, non-polarizable spheres.
- A polyhedron of anions will be formed around cations and vice-versa.
- The coordination number will be the maximum determined by ionic radii.
- Around the ions (cations or anions) site electroneutrality must be preserved.
- The coordinating ions are arranged so as to minimize the electrostatic repulsive energy.

Most economical use of space is controlled by atomic size or ionic radius. Moreover, some apparent trends observed by Greenwood are worth mentioning.

- Cations are normally smaller than anions, the only exception being Rb^+, Cs^+, Fr^+ and Ra^+, which are larger than smallest anion F^-.
- Within the vertical group of the Periodic Table the radius increases with the atomic number.
- Within each iso-electronic sequence in the PT the radius decreases rapidly with increase in positive charge, e.g., 0.75 Å for Na^+ and 0.26 Å for Cl^{7+}.
- Successive increase in valancy of cation progressively decreases its radius.

Table 6.2 Type of structural arrangement and radius ratio [3].

Coordination Arrangement	Symmetry of Anion around Cation	Coordination Number	ρ'
Cubic	Corners of cube	8	1–0.732
Octahedron	Corners of regular octahedron	6	0.732–0.414
Tetrahedron	Corners of regular tetrahedron	4	0.414–0.225
Trigonal Planar	Corners of equilateral triangle	3	0.225–0.155
Linear	Linear	2	0.155–0

Crystal structure is determined by the number of anions while it is possible to pack around the smaller cation. A different type of coordination arrangement is obtained for different values of radius ratio . Table 6.2 depicts a few examples.

$$\rho' = \frac{r_{cation}}{r_{anion}} \tag{6.11}$$

6.3 Classification of Solid Electrolytes

The solid electrolytes are classified on the basis of various aspects, a few of which are discussed below.

Based on the conducting ion species of the SE these materials are classified as cationic SE and anionic SE. Further, depending upon the number of charge carriers involved in the conduction process, SE may be subclassified as unipolar and bipolar SE. If the conducting carriers are more than one, and all are cations or anions, the SE is categorized as unipolar SE. However, if the carriers are mixed, i.e., cations and anions, then that material is categorized as bipolar SE.

Factors responsible for conduction processes also influence the classification scheme. One may refer to the kind of commonly studied defects, like Frenkel and Schottkey, for classification of SE such as F-type and S-type SE. The kind of doping in the host material also gives rise to classes like iso-valent, monovalent, di-valent, trivalent or in general alio-valent SE. As the nomenclature suggests,

doping a system with singly charged cation, doubly charged cation, and triply charged cation gives rise to monovalent, divalent and trivalent SE, respectively. When a mono-valent system is doped with mono-valent system or di-valent system is doped with di-valent system then the resultant system is iso-valent SE.

Based on the nature of the system, the materials are also classified into crystalline SE (single/poly), amorphous SE, composite SE, polymer SE, glass SE, etc. This classification scheme may further evolve with time as the materials research progresses into newer regimes.

6.4 Criteria for High Ionic Conductivity and Mobility

In a SE, ions can hop in solid, and thereby contribute to ionic conductivity only if their immediate environment includes vacant site which is energetically accessible. Ion hopping depends upon:

- Number of available vacant sites in the immediate vicinity of the ion.
- Modest energy barriers between the nearby vacant site.

Moreover, the third condition for appreciable long-range motion of the ions is that:

- There must be interconnected ion migration paths through the lattice (hop without significant drift avoided). This resembles the game of Chinese Checkers in which one encounters a special condition wherein the marble finds a long hopping path that leads to its destination.

The expression for conductivity derived by considering the hopping mechanism is a product of the fractional number of defects and the hopping rate (hopping frequency):

$$\sigma = Av_d n_d = A\ exp\left(-\frac{E_f}{k_B T}\right) exp\left(-\frac{E_m}{k_B T}\right) \qquad (6.12)$$

Here, E_f and E_m represent formation energy per defect and barrier height for hopping (ion migration enthalpy), respectively.

In addition to the above considerations, fast ion transport in SE results at the same time from microscopic properties connected to chemical bonding in the material and its structural features. Reviewing the characteristics of a number of SEs within the framework of their structural aspects, Reau *et al.* [6] have formulated the following important criteria for high ionic conductivity/mobility in solids:

1. Small ionic radius and charge on the mobile ion
2. High ionic polarizability of constituent ions
3. Weak binding energy between mobile and antagonist ions
4. Low coordination number of mobile ions
5. Low melting point

The ionic conductivity in SE is related to concentration of charge carriers (η) and their mobility (μ) by a well-established relation:

$$\sigma = nq\mu \qquad (6.13)$$

6.5 Electrical Characterization of Solid Electrolyte

The electrical characterization of the SE is one of the prime characterizations that can establish (*i*) whether the conductivity is contributed by mobility of ions or electrons or both, and (*ii*) the conductivity (S/cm) of the specimen is independent of its physical dimensions.

6.5.1 DC Polarization

To establish whether the conductivity is due to ions or electrons, the material being tested is obtained in the regular geometry, placed between two electrodes and excited by a dc source. The dc potential should be below the decomposition potential as; (-)M/MX/Inert electrode(+) (III).

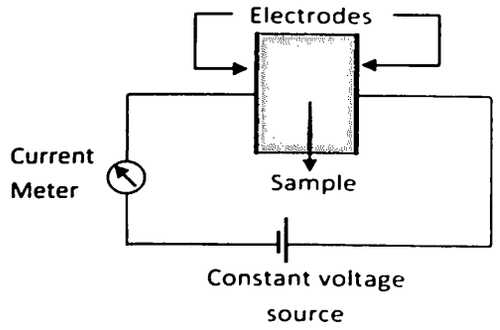

Figure 6.2 Schematic diagram of ionic transport measurement setup.

The schematic diagram in Figure 6.2 represents the ionic transport measurement setup. This setup is used to measure circuit current as a function of time. The electronic resistance is unchanged by the dc polarization potential, however, the ionic resistance decreases with time as the polarization builds up. Danforth and Bodine [7] and Vest and Tallan [8] have derived the following formula:

$$t_i = \frac{\sigma_0 - \sigma_\infty}{\sigma_0} \tag{6.14}$$

In the case where the conductor is a mixed one, i.e., the conductivity is contributed by ion transportation as well as electrons, we can write:

$$\sigma = \sigma_i + \sigma_e$$

$$1 = \frac{\sigma_i + \sigma_e}{\sigma} = \frac{\sigma_i}{\sigma} + \frac{\sigma_e}{\sigma} = t_i + t_e \tag{6.15}$$

where σ_i, σ_e, are conductivity contributions of ion and electrons, respectively, and t_i, t_e represent the ionic and electronic transport number.

Figure 6.3 represents a typical time-dependent plot of conductivity frequently reported in the literature [9] of SE. For a perfect electronic conductor, the conductivity will be independent of time, i.e., a line parallel to time axis. For a perfect mixed conductor, the ionic and electronic transport number will be $t_i = t_e = 0.5$. It clearly shows that with time the polarization grows, thereby squeezing the total (ionic + electronic) conductivity to only electronic.

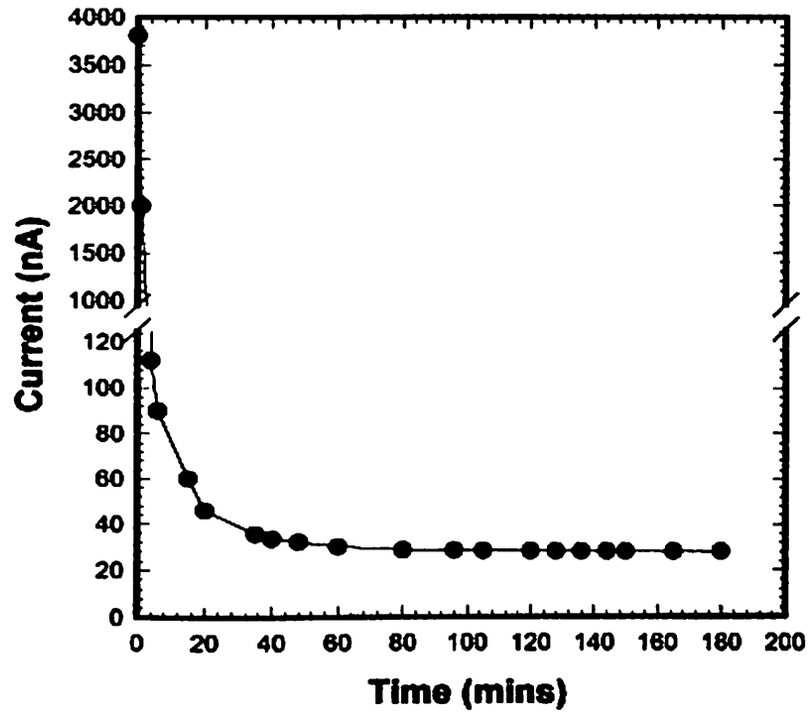

Figure 6.3 Typical time-dependent conductivity plot.

6.5.2 Impedance Spectroscopy

The complex impedance spectroscopic study involves measurement of real and imaginary parts of impedance as a parametric function of a wide range of frequency. This technique has become a fundamental tool to determine physical parameters like ionic conductivity, electrode polarization and activation enthalpy for ion migration.

In usual representations, the voltage, current and impedance may be represented as:

$$V(t) = V_m e^{j\omega t}, I(t) = I_m e^{j\omega t - \varphi}$$

$$Z = Z_r - jZ_i, Z = \sqrt{Z_r^2 + Z_i^2}, \varphi = arc\left(\tan\frac{Z_i}{Z_r}\right) \tag{6.16}$$

The frequency-dependent impedance will be:

$$Z(\omega) = Z(0) + \frac{Z(\infty) - Z(0)}{1 + (j\omega\tau)^a} \tag{6.17}$$

where $Z(0)$ and $Z(\infty)$ are limiting values of $Z(\omega)$ when ω varies from minimum to maximum, τ is relaxation time, and α is empirical measure of departure from ideal Debye model. During the non-linear least square fitting (NLS) fitting the sum of squares is minimized by unity weighing represented by:

$$S_i = (\Delta R_i)^2 + (\Delta I_i)^2 \tag{6.18}$$

where ΔR_i and ΔI_i are the real and imaginary fitting residuals. The presence of two overlapping depressed semicircular arcs is suggestive of the occurrence of two prominent conduction mechanisms simultaneously under the external perturbation ac signal. Various interpretations can be made in the impedance analysis in a polycrystalline ion conducting specimen; however, an experimental impedance obviously contains major contributions from inter-grain and intra-grain ion migration [10,11]. In order to have a more meaningful discussion, the voluminous impedance data obtained by following the above procedure are fitted into the equation:

$$f_p = f_0 e^{-E_m/kT} \tag{6.19}$$

The peak frequency of the complex impedance $\omega_{max} = 2\pi f_p$

$$\frac{1}{\tau} = \frac{1}{RC} = \frac{\sigma}{\varepsilon a \mu C} \cdot \mu = \mu_0 e^{-E_m/kT} \tag{6.20}$$

where μ is the cationic mobility, E_m denotes the migration enthalpy, μ_0 is proportional to the jump attempt frequency, and k and T are the Boltzmann constant and temperature in K. The frequency f_p derived from ω_{max} is an effective averaged hopping frequency of an ion. The effective pre-factor f_o depends on the defect charge carrier density, C.

The process of ion migration through the sample involves the activation energy for migration of ions across the grain boundaries, E_{a2} (obtained from the semicircle corresponding to high frequency), and that for migration of ions within grain (intra-grain) ion migration, E_{a1} (obtained from the semicircle corresponding to low frequency).

In the complex impedance plot real and imaginary impedance has been plotted as a parametric function of frequency and a trendy behavior as shown in Figure 6.4. The low frequency intercept of the arc on real axis represents bulk resistance.

$$\text{Resistivity} \quad \rho = \frac{R_{bulk} A}{l} \tag{6.21a}$$

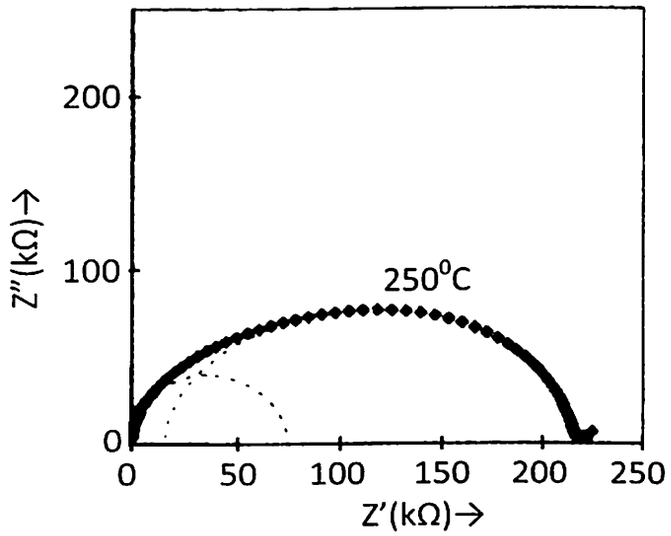

Figure 6.4 Complex impedance plot for pure Ag_2SO_4 at 250°C (the dotted line represents the best fit curve).

$$\text{Conductivity} \quad \sigma = \frac{l}{R_{bulk} A} \tag{6.21b}$$

Such typical plots possess an equivalent electrical circuit as these circuits yield similar plots. This has been extensively studied by Pande *et al.* and a tradition of depicting equivalent circuit for SE has grown up as a way of describing features of the SE [12].

Figure 6.5 shows a typical complex impedance plot of real and imaginary impedance as a parametric function of frequency (ω). The bulk resistance, constant phase element (CPE) and resistance combinations for a typical equivalent circuit are also shown.

6.6 Ionic Conductivity and Temperature

The generalized perception of the Arrhenius theory of the temperature effect on the reaction rate (ion diffusion) originated from the temperature effect on the equilibrium constant. It is known that:

$$\frac{d\ln(K)}{d\frac{1}{T}} = -\frac{H}{R} \tag{6.22}$$

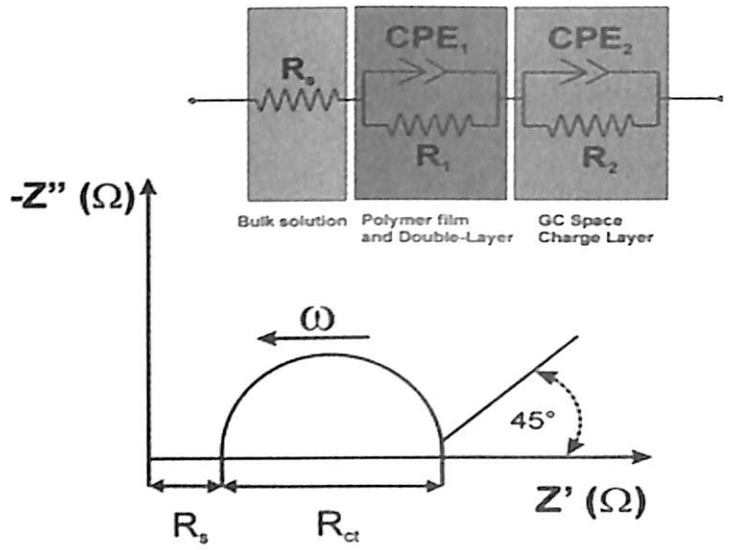

Figure 6.5 Complex impedance plot and typical equivalent circuit.

where K is an equilibrium constant, R is the gas constant, and H is the heat of reaction. The equilibrium constant is $= \frac{k_1}{k_2}$, where k_1 and k_1 are the rate constants for the forward and reverse reactions respectively. Thus, we obtain:

$$\frac{dln(k_1)}{d\frac{1}{T}} - \frac{dln(k_2)}{d\frac{1}{T}} = -\frac{H}{R} \tag{6.23}$$

Arrhenius recognized that the last equation could be conveniently divided into two parts, each having the form of –

$$\frac{dln(k)}{d\frac{1}{T}} = -\frac{E}{R} \tag{6.24}$$

where E is referred by Arrhenius as representing the energy difference between the reactants and an activated species. The term E is, therefore, called the activation energy. Taking E as a constant the last can be integrated to yield:

$$\ln(k) = \ln(A) - \frac{E}{RT} \tag{6.25}$$

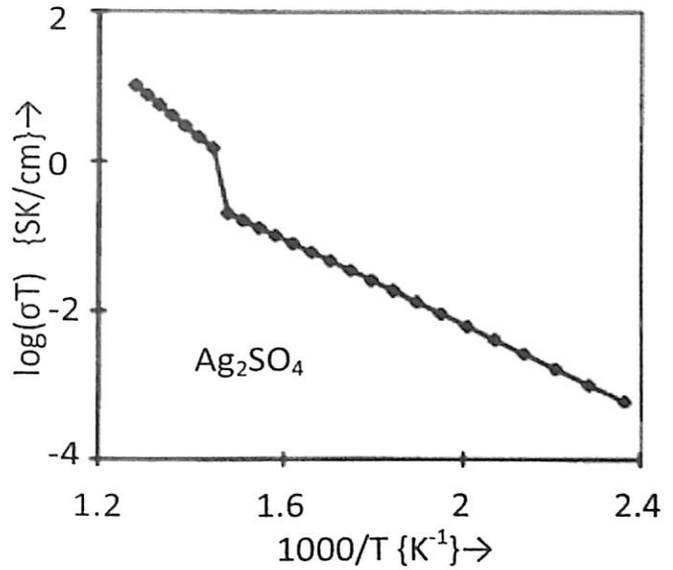

Figure 6.6 Arrhenius plot for SE (pure Ag_2SO_4 in β hexagonal and orthorhombic phase).

where $ln(A)$ is the constant of integration and the last equation can be converted to:

$$k = Ae^{-\frac{E}{RT}} \tag{6.26}$$

This form of Eq. 6.26 is the most widely adopted form of the Arrhenius equation. The temperature-dependent ionic conductivity in all specimens as governed by Arrhenius equation can be expressed as Eq. 6.27.

$$(\sigma T) = (\sigma T)_o \exp\left(\frac{E_a}{2KT}\right) \tag{6.27}$$

The pre-exponential factor $(\sigma T)_0$ in the above equation (which is appearing out of constant of integration) is related to the frequency of ionic collisions in the collision theory and to the entropy term in the transition state theory. The equation governs forward and reverse reaction contributing to ionic conductivity (σT) and predomination of each other. Arrhenius plots for all the compositions are found to obey the Arrhenius law (25) in both the α and β phases (as an example, Figure 6.6 depicts this behavior for the host Ag_2SO_4).

The observed change in slope at 416°C with an order of magnitude jump in conductivity in the case of pure Ag_2SO_4 accounts for the orthorhombic β to hexagonal α phase transition (Figure 6.6). The magnitudes of the conductivities (2.22×10^{-3} S/cm at 250°C and 3.4×10^{-3} S/cm at 440°C) and the transition temperature (416°C) are in close agreement with earlier reports [13–16].

6.7 Concentration-Dependent Conductivity

The concentration of mobile charge carriers in a Frenkel type ionic solid is given by:

$$n = \sqrt{k_f}\exp\left(\frac{\Delta S_{th} + \Delta S_{cf}}{2k} - \frac{E_f}{kT}\right) \tag{6.28}$$

where k_f, ΔS_{th}, ΔS_{cf} and E_f are, respectively, the mass action constant, thermal entropy, configurational entropy and defect formation enthalpy. If the system under consideration (solid solution of Ag_2SO_4 with Me_2SO_4) is assumed to be homogeneous and isotropic, then the term ΔS_{cf} remains invariant with respect to the distribution of cations and anions, whereas the immediate ions surrounding Me^+ will have a different vibrational frequency v' from those at regular undistorted sites v. The thermal entropy term ΔS_{th} in the last equation will be a consequence of the change in frequency of the lattice vibration due to the distortion taking place. Considering the Einstein model we may assume that in the doped crystal, each atom neighboring Me^+ is equivalent to three harmonic oscillators each of frequency $v' \neq v$. Then one finds for the increase in thermal entropy per Me^+ the expression,

$$\Delta S_{th} = 12k\log\left(\frac{v}{v'}\right) \tag{6.29}$$

substitution of which in last Eq. 6.13 leads to:

$$n = k_f\left(\frac{v}{v'}\right)^6\exp\left(-\frac{E_f}{2kT}\right) \tag{6.30}$$

6.8 Ionic Conductivity in Composite SE

Composite materials are heterogeneous mixtures of solid phases. The elaboration of composites offers a new degree of freedom in the search for advanced functional materials, because specific properties can be tailored to a certain degree by mixing appropriate phases. In the domain of solid-state ionics, two routes can lead to improved solid ionic conductors: a search for new compounds and structures sustaining high levels of ionic conductivity or a modification of existing compounds by heterogeneous or homogeneous doping. The latter involves homogenous dissolution of a certain amount of aliovalent dopant in the bulk of the ionic conductor M^+X^- in order to increase the concentration of mobile charge carriers according to bulk defect equilibrium. One example is the creation of additional vacancies by doping with cations of higher valence, such as D^{2+} in substitution of M^+, written in KroÈger-Vink nomenclature [17–26]:

$$DX_2 + 2M_M \rightarrow D_M^{\cdot} + V_M^{'} + 2MX \tag{6.31}$$

Heterogeneous doping, on the contrary, involves mixing with a second phase with very limited solid solubility and the formation of defect concentration profiles in the proximity of interfaces. The deviations from local electrical neutrality (space charges) are a consequence of point defect equilibrium at interfaces [27]. Apart from the improvement of the electrical properties, such as high conductivity and ionic transference number, the development of composite materials can also lead to better mechanical properties, such as better shock resistance or higher strength. Although composite materials can in principle contain many different phases, literature in the field of solid-state ionics deals primarily with two-phase mixtures. In 1973, Liang [28] observed an enhancement of ionic conductivity by a factor of almost 50 in a composite material made from lithium iodide LiI, a compound with moderate Li ion conductivity at ambient temperature, and dispersed small alumina Al_2O_3 particles. The maximum lay around 40 vol% alumina. After this initial study, the conductivity enhancement in heterogeneous materials was confirmed for numerous ceramic composites, including dispersions of fine insulator particles in an ionic conductor matrix and mixtures of two different ionic conductors, with a major contribution by J.B. Wagner and his group [29]. The majority of the study was

conducted on monovalent cation conductors, such as lithium, silver and copper halides, the largest group being lithium compounds, given their importance in high energy density portable batteries. Besides Al_2O_3, other oxides, such as MgO, SiO_2, CeO_2, TiO_2 and ferroelectric $BaTiO_3$, were found to be effective second phases for ionic conductivity improvements.

More recently, the composite effect was also observed in ceramic anion conductors, such as lead or calcium fluoride, and even in inorganic solids with trivalent cation conductivity, like aluminum and rare-earths. The theory of ionic conductor composites, which was developed in the first part, highlights the importance of phase boundaries for the electrical properties. Boundaries can be transport pathways or transport barriers, given their modified core structure (core effects), and can effect the charge carrier distribution in the adjacent regions (space charge effects). Local deviations from electrical neutrality in the vicinity of interfaces were recognized a long time ago in the electrochemistry of liquid electrolytes or in colloidal systems. Gouy [30] established the theory of the electrical double layer at the electrode-electrolyte interface in 1903, and Overbeek and coworkers [31] the electrostatic colloid theory in 1948. In 1953, Lehovec [32] calculated the defect distribution at the surface of ionic crystals and discussed the implications for ionic conduction. In 1972, Wagner [33] used the space charge layer concept to explain conductivity effects in two-phase materials with electronic conduction, such as metallic inclusions in a semiconducting oxide or mixtures of two semiconducting oxides. After an attempt by Jow and Wagner in 1979 [34], the space charge layer theory of heterogeneous ionic conductors was established by Maier [35,36] after 1984. So far, ceramic composites, which are mixtures of two crystalline inorganic phases, represent the most important group in solid-state ionics. However, a growing amount of work was recently devoted to glass-ceramic composites obtained by partial crystallization of a glassy matrix, and polymer-ceramic composites, where an inorganic compound is dispersed in a polymer matrix. Agrawal and Gupta [37] reviewed composite solid electrolytes and gave an extensive list of systems reported in the literature.

Silver sulphate, a non-alkali metal sulphate, is also an exception which shows high cationic conductivity in spite of the bigger size of Ag^+. It undergoes a structural phase transition from the high temperature highly conducting hexagonal α-phase to the low temperature moderately conducting orthorhombic β-phase

at 416°C. It attracted attention until its potential application in SO_x (x=2, 3) galvanic sensors was proved [38]. Ever since the concept of using a metal/metal sulphate reference electrode in solid electrochemical gas sensors has evolved, it has attracted a great deal of attention. It exhibits many advantages over other sulphate-based [39] solid electrolytes in engineering SO_2 gas sensors like: (*i*) coexistence of Ag–O–S phase in Ag/Ag_2SO_4; (*ii*) equilibration of antagonist SO_4^{2-} (solid) with SO_2/SO_3 (gas); (*iii*) invariance of high ionic conductivity over the SO_x environment, etc. [40–49].

Figure 6.7 shows schematic grain boundary consisting of a positive core charge compensated by two adjacent space–charge layers. Values of x are defined such that $x = 0$ at the interface between the space–charge layer and the grain boundary core, while far into the grain interior $x = \infty$. The dotted lines represent concentration profiles in the space–charge layer for the protons and the acceptor dopant under the Mott–Schottky approximation, while the unbroken line represents the potential profile. The Schottky barrier height potential difference is also indicated.

Interfaces play an important role for the transport properties of polycrystalline and poly-phase (composite) materials. Given the anisotropy of boundaries, one has to distinguish between transport along and across interfaces. Enhanced ionic conduction along interfaces can be observed for two reasons. First, the interface core itself is a disordered region, where defect formation and migration energies are generally notably reduced. This leads to

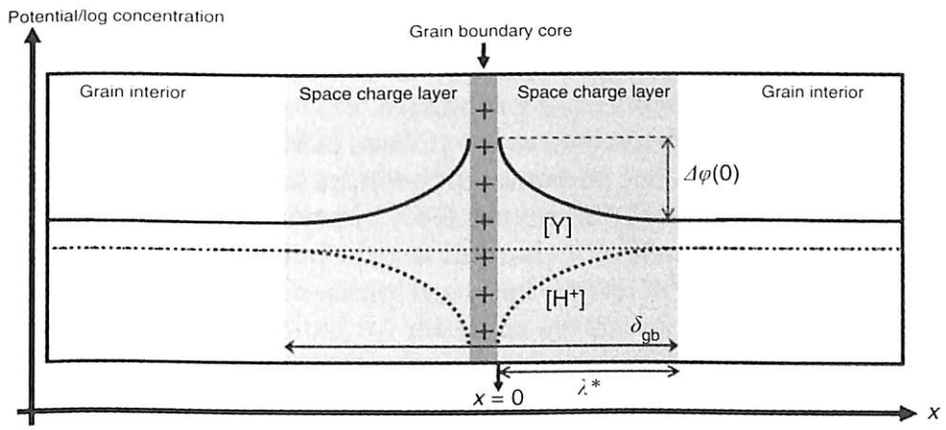

Figure 6.7 Schematic grain boundary representation of potential and concentration.

enhanced ionic transport within the interface core (grain boundary diffusion). However, core effects are generally small, given the reduced interface area in conventional microcrystalline materials. Some studies established the role of grain boundary diffusion in polycrystalline oxides, including NiO, Al_2O_3, MgO [50] or ZnO [51], but there seems to be no similar study in composite materials. Second, point defect and dopant interactions with interfaces, for example, accumulation in the interface core (intrinsic and extrinsic interfacial segregation), induce concentration profiles of point defects in the regions adjacent to the interface in ionic materials (space charge layers). Only few quantitative studies exist on grain boundary segregation in oxides, including CaO-doped ZrO_2 [52], TiO_2 [53] and CeO_2 [54], and similar studies on phase boundaries in composite materials are even more difficult, from an experimental as well as a theoretical point of view. The concentration profiles of mobile charge carriers near interfaces are a consequence of thermodynamic defect equilibrium.

6.9 Thermodynamics of Electrochemical System

The thermodynamics of electrochemical system deals with a difference in electric potential between two or more phases. Electric forces, fields, potentials and potential energy are important not only in the thermodynamics but throughout chemistry. The properties of an atom or a molecule are the result of electrical interactions. To write a fundamental equation for such a microscopic system, say the Schrodinger equation, we need to know the equation for the potential energy of interaction between charges. Forces between molecules are also electrical in nature. However, dipole moment and polarizability determines properties.

In an electrochemical system, the phases normally have non-zero net charges, and electric potential differences exist between phases. These electric potential differences (PD) are typically a few volts or less. How much transfer of charged matter between phases occurs when PD of, say, $10V$ exists between phases? To get an order of magnitude of the answer, we consider an isolated spherical phase of radius 10 cm that is at an electric potential of $\varnothing = 10\ V$. Let Q be the net charge on the phase. The electric potential at the edge of the phase of radius r is given by $\varnothing = Q / 4\pi\varepsilon_0 r$, and

$$Q = 4\pi\varepsilon_0 r\varnothing = 4\pi\left(8.85\times10^{-12}C^2N^{-1}m^{-2}\right)(0.1m)(10V) = 1\times10^{-10}C \quad (6.32)$$

Suppose this charge is due to an excess of Cu^{2+} ions. We have $Q_i = Z_i F n_i$. And amount of excess Cu^{2+} is

$$n_i = \frac{Q_i}{Z_i F} = \frac{1\times10^{-10}C}{2\times96485C/mol} = 5\times10^{-16}mol \quad (6.33)$$

which is a mere 3×10^{-14} gm of Cu^{2+}. Thus, we conclude that the net charges of phases of electrochemical systems are due to transfers of amounts of matter far too small to be detected chemically. However, a countable potential 10 V is worthwhile.[1]

The presence of PDs between phases affects the thermodynamic equations because the internal energy of a charged species depends on the electric potential of the phase it is in. When the phases of an electrical system are brought together to form the system, tiny amounts of charge transfer between the phases produce PDs between phases. Imagine a hypothetical system in which these charge transfers have not occurred, so that all the phases have an electric potential of zero: $\varnothing^\alpha = \varnothing^\beta = \ldots = 0$. If we add db_j moles of j to phase α of this hypothetical system, the Gibbs equation gives the change in internal energy phase α as:

$$dU^\alpha = TdS^\alpha - PdV^\alpha + \mu_j^\alpha dn_j^\alpha \text{ for } \varnothing^\alpha = 0 \quad (6.34)$$

All terms carry usual meaning, dnj is function of T, P and composition of phase: $\mu_j^\alpha = \mu_j^\alpha(T, P, x_1^\alpha, x_2^\alpha \ldots)$.

Now consider the actual system in which charge transfers between phases do occur to produce phases with electric potentials $\varnothing^\alpha, \varnothing^\beta, \ldots$. As discussed earlier, these charge transfers correspond to negligible amount of chemical species, so that we can consider each phase of the actual electrochemical system to have the same

1 The effective species parameter Coulomb Per Mol (C/mol) is a unit in the category of *Molar electric charge*. It is also known as coulombs/mol. Coulomb Per Mol (C/mol) has a dimension of $TN^{-1}I$ where T is time, N is amount of substance, and I is electric current. This unit is the standard SI unit in this category.

composition as the corresponding phase of the hypothetical system, with the electric potential equal to zero. Thus we can write,

$$dU^{\alpha} = TdS^{\alpha} - PdV^{\alpha} + \mu_i^{\alpha} dn_i^{\alpha} + \varnothing^{\alpha} dQ_i^{\alpha}$$

$$dU^{\alpha} = TdS^{\alpha} - PdV^{\alpha} + \sum_i \left(\mu_i^{\alpha} + Z_i F\varnothing^{\alpha}\right) dn_i^{\alpha}$$

$$dU^{\alpha} = TdS^{\alpha} - PdV^{\alpha} + \sum_i \tilde{\mu}_i^{\alpha}\, dn_i^{\alpha} \quad \text{for } \tilde{\mu}_i^{\alpha} = \left(\mu_i^{\alpha} + Z_i F\varnothing^{\alpha}\right) \qquad (6.35)$$

The above equation shows that the presence of non-zero electric potential $\varnothing^{\alpha}$ in the phase α causes the chemical potential μ_i^{α} to be replaced by $\left(\mu_i^{\alpha} + Z_i F\varnothing^{\alpha}\right)$ in Gibbs equation for dU^{α}. This quantity $\tilde{\mu}_i^{\alpha} = \left(\mu_i^{\alpha} + Z_i F\varnothing^{\alpha}\right)$ is known as electrochemical potential.

In a closed system, the equilibrium condition for two phases α and β in contact is $\tilde{\mu}_i^{\alpha} = \tilde{\mu}_i^{\beta}$ for each substance i present in both phases. In closed electrochemical system, the reaction equilibrium condition is $\sum_i \nu_i \tilde{\mu}_i = 0$. Here, ν_i's are stoichiometric coefficients of reaction.

6.10 Applications

Solid electrolytes (SE) have attracted a great deal of attention due to their high potential for applications in various devices that include sensors, batteries, thermal batteries, heart pacemakers, smart windows, etc. Some of these applications will be discussed in this section.

6.10.1 Solid-State Batteries

An electrochemical cell consists of two half-cells. Each half-cell consists of an electrode, and an electrolyte. The two half-cells may use the same electrolyte, or they may use different electrolytes. The chemical reactions in the cell involve the electrolyte, the electrodes or an external substance (as in fuel cells, which may use hydrogen gas as a reactant). In a full electrochemical cell, species from one half-cell lose electrons (oxidation) to their electrode, while species from

the other half-cell gain electrons (reduction) from their electrode. A salt bridge (e.g., filter paper soaked in KNO_3) is often employed to provide ionic contact between two half-cells with different electrolytes, to prevent the solutions from mixing and causing unwanted side reactions in most of the cells involving liquid electrolytes. As electrons flow from one half-cell to the other, a difference in charge is established. If no salt bridge was used, this charge difference would prevent further flow of electrons. A salt bridge allows the flow of ions to maintain a balance in charge between the oxidation and reduction vessels, while keeping the contents of each separate. Other devices for achieving separation of solutions are porous pots and gelled solutions. A porous pot is used in the Bunsen cell.

Each half-cell has a characteristic voltage. Different choices of substances for each half-cell give different potential differences. Each reaction is undergoing an equilibrium reaction between different oxidation states of the ions: when equilibrium is reached, the cell cannot provide further voltage. In the half-cell which is undergoing oxidation, the closer the equilibrium lies to the ion/atom with the more positive oxidation state, the more potential this reaction will provide. Similarly, in the reduction reaction, the closer the equilibrium lies to the ion/atom with the more negative oxidation state, the higher the potential.

The cell potential can be predicted through the use of electrode potentials. These half-cell potentials are derived from the assignment of 0 volts to the standard hydrogen electrode. The difference in voltage between electrode potentials gives a prediction for the potential measured. When calculating the difference in voltage, one must first manipulate the half-cell reactions to obtain a balanced oxidation-reduction equation.

1. Reverse the reduction reaction with the smallest potential (to create an oxidation reaction/overall positive cell potential).
2. Half-reactions must be multiplied by integers to achieve electron balance.

It is important to note that the cell potential does not change when the reaction is multiplied.

Cell potentials have a possible range of about 0 to 6 volts. Cells using water-based electrolytes are usually limited to cell potentials less than about 2.5 volts, because the very powerful oxidizing and

reducing agents which would be required to produce a higher cell potential tend to react with the water.

6.10.1.1 *Energy Issues*

During operation of electrochemical cells, chemical energy is transformed into electrical energy and is expressed mathematically as the product of the cell's emf and the electric charge transferred through the external circuit.

$$Electrical\ Energy = E_{cell} C_{trans} \tag{6.36}$$

where E_{cell} is the cell potential measured in volts (V) and C_{trans} is the cell current integrated over time and measured in coulombs (C); C_{trans} can also be determined by multiplying the total number of electrons transferred (measured in moles) times Faraday's constant (F).

The emf of the cell at zero current is the maximum possible emf. It is used to calculate the maximum possible electrical energy that could be obtained from a chemical reaction. This energy is referred to as electrical work and is expressed by the following equation:

$$W_{max} = W_{electrical} = -nFE_{cell} \tag{6.37}$$

where work is defined as positive into the system.

Since the free energy is the maximum amount of work that can be extracted from a system, one can write:

$$\Delta G = -nFE_{cell} \tag{6.38}$$

A positive cell potential gives a negative change in Gibbs free energy. This is consistent with the cell production of an electric current from the cathode to the anode through the external circuit. If the current is driven in the opposite direction by imposing an external potential, then work is done on the cell to drive electrolysis.

A spontaneous electrochemical reaction (change in Gibbs free energy less than zero) can be used to generate an electric current in electrochemical cells. This is the basis of all batteries and fuel cells. For example, gaseous oxygen (O_2) and hydrogen (H_2) can be combined in a fuel cell to form water and energy, typically a combination of heat and electrical energy.

Conversely, nonspontaneous electrochemical reactions can be driven forward by the application of a current at sufficient voltage. The electrolysis of water into gaseous oxygen and hydrogen is a typical example.

The relation between the equilibrium constant, K, and the Gibbs free energy for an electrochemical cell is expressed as follows:

$$\Delta G^0 = -RTln(k) = -nFE^0_{cell} \tag{6.39}$$

Rearranging to express the relation between standard potential and equilibrium constant yields:

$$E^0_{cell} = \frac{RT}{nF}\ln(k) \tag{6.40}$$

The previous equation can use Briggsian logarithm as shown below:

$$E^0_{cell} = \frac{0.0591V}{n}\ln(k) \tag{6.41}$$

6.10.1.2 *Nernst Equation*

The standard potential of an electrochemical cell requires standard conditions for all of the reactants. When reactant concentrations differ from standard conditions, the cell potential will deviate from the standard potential. In the 20th century, German chemist Walther Nernst proposed a mathematical model to determine the effect of reactant concentration on electrochemical cell potential.

In the late 19th century, Josiah Willard Gibbs formulated a theory to predict whether a chemical reaction is spontaneous based on the free energy:

$$\Delta G = \Delta G^0 + RTln(k) \tag{6.42}$$

Gibbs' key contribution was to formalize the understanding of the effect of reactant concentration on spontaneity.

Based on Gibbs' work, Nernst extended the theory to include the contribution from electric potential on charged species. As shown in the previous section, the change in Gibbs free energy for an electrochemical cell can be related to the cell potential. Thus, Gibbs' theory becomes:

$$nF\Delta E = nF\Delta E^0 - RTln(k) \tag{6.43}$$

Here n is the number of electrons/mole product, F is the Faraday constant (coulombs/mole), and ΔE is cell potential. Finally, Nernst divided through by the amount of charge transferred to arrive at a new equation which now bears his name:

$$\Delta E = \Delta E^0 - \frac{RT}{nF} \ln(k) \tag{6.44}$$

Assuming standard conditions (T = 25°C) and R = 8.3145 J/(K·mol), the equation above can be expressed as shown below:

$$\Delta E = \Delta E^0 - \frac{0.05916}{n} (\log k) \tag{6.45}$$

This form of Nernst equation is valid for electrolytes which are even in solid state. And a similar form of equation may be extended for solid batteries after accounting for the chemical/electrochemical potentials in the basic equations.

6.10.2 Sensors

According to the Nernst equation, all metal and hydrogen has a tendency to pass into solution in the form of ions; e.g., zinc metals when immersed into pure water liberate Zn^{2+} into water under stress of solution pressure as:

$$Zn \rightarrow Zn^{2+} + 2e^- \tag{6.46}$$

and the metal is left negatively charged due to loss of Zn^{2+}. As these charges are massive, they do not move away from oppositely charged metal, thus forming an electrical double layer at the junction of electrode and electrolytic solution. The layer builds up as more and more positive charges go into the solution. Now, if one considers a metal electrode dipped in the solution of its own salt, the tendency of ions to pass into the solution is opposed by the reverse tendency of ions to be deposited back on the electrode. This backward reaction is attributed to osmotic pressure of ions in the solution. Thus the potential difference between the metal and the solution of its salt depends upon two facts, viz. (a) tendency of metal ions to pass into solution (solution pressure) and (b) the

tendency of metal ions in the solution to be deposited on electrode (osmotic pressure). Thus depending upon relative magnitudes, there are three possibilities:

a) *Solution pressure > Osmotic Pressure*

Tendency of ions to leave metal will be greater than reverse tendency and metal will be left negatively charged with respect to electrolyte solution, e.g., Zn, Cd and alkali metals.

b) *Solution pressure < Osmotic pressure*

Tendency of ions to get deposited on metal will be greater than reverse tendency and metal will gain positive charge with respect to electrolyte solution, e.g., Cu, Au, Ag and Hg.

c) *Solution pressure = Osmotic pressure*

Both processes are balanced, no layer is formed and no potential difference is developed between metal and solution resulting in null electrode.

6.10.2.1 Nernst Equation

Consider a metal of valance n, P_1 and P_2 represents osmotic and solution pressure respectively, and E represents actual potential difference between metal and solution. An electric current is passed through electrode reversibly until 1g ions of metal are dissolved. The quantity of electricity required for the dissolution of 1g of metal ions will be nF Coulombs.

$$\textit{The electric workdone} = nFE \text{ Volts-Coulombs} \tag{6.47}$$

(where F = 96,500 coulombs). Now suppose that the solution is diluted so that the osmotic pressure is reduced from P_1 to $P_1 - dP_1$. The corresponding difference of potential between the metal and the solution is now changed from E, to say, dE.

Now, in order to cause dissolution of 1 g ions of metal, the electrical work done or electrical energy to be expensed is $(E - dE)nF$ volt-coulomb.

The difference between electrical energy =
$$nEF - (E - dE)nF = dEnF \tag{6.48}$$

The difference between electrical energy must be equal to the osmotic work done in transferring 1 g of ions of the metal from P_1 to $P_1 - dP_1$.

$$\text{The work done} = VdP_1 \tag{6.49}$$

here V is volume of the solvent. Therefore,

$$dEnF = VdP_1 \tag{6.50}$$

$$dEnF = \frac{RT}{P_1} dP_1 \text{ as } \frac{RT}{P_1} = V \tag{6.51}$$

Integrating and finding the constant of integration for equilibrium condition at $P_1 = P_2$, $E = 0$ one gets

$$E = \frac{RT}{nF} \log\left(\frac{P_1}{P_2}\right) \tag{6.52}$$

Now if two similar electrodes are dipped in two different solutions, say A and B, the pd between the two electrodes will be:

$$E_1 - E_2 = \frac{RT}{nF} \log\left(\frac{P_{A1}}{P_{B2}}\right) \tag{6.53a}$$

As osmotic pressure is directly proportional to concentration, we can rewrite the above equation as:

$$E_1 - E_2 = \frac{RT}{nF} \log\left(\frac{C_{A1}}{C_{B2}}\right) \tag{6.53b}$$

6.10.3 SO_2 Sensor Kinetics and Thermodynamics

Sulphate-based solid electrolytes (SEs) have attracted a great deal of attention [55] due to their high potential of applications in various devices that include sensors, batteries, thermal batteries, heart pacemakers, smart windows, etc. In the process of modernization and industrialization that has developed around mankind to facilitate

life, unwanted pollutants have grown up. Nowadays the pollutants have created sizeable destruction. Detecting and monitoring the pollutants have become an objective to support and sustain healthy life on the planet. Sulpher dioxide (SO_2) is one such harmful known pollutant that has been counter-attacked by human beings for a long time [56–58]. In earlier times it was detected by gas chromatography. This methodology is obsolete and redundant now. In the present context of modernization, the detection techniques should be fast, automatic and electronically compatible for PC interface.

In earlier stages of development, gaseous reference electrode was used which was cumbersome to handle and measurements interfering. The innovative solid reference electrode (Ag+Ag2SO4) [46] has proved advantageous over reference gas electrode. The quality performance of solid-state electrochemical gas sensor (SSEGS) in terms of response time, thermodynamic stability, operating temperature, gas sensing ability, sensitivity and concentration range that is sensed has evoked in Test gas-cathode/solid electrolyte/reference anode cell assemblyterest [59]. The sensor configuration is described below.

Test Gas Cathode/Solid Electrolyte/Reference Anode Cell Assembly

The cell with configuration Ag:Ag_2SO_4/*SE*/Pt, SO_2(g), O_2(g) was fabricated by simultaneously pressing the reference electrode and electrolyte. On the other side, Pt powder was sprinkled to derive electrical contact. The sensor cell is embedded into graphite as shown in Figure 6.8.

The half-cell reaction at the electrolyte gas interface is the equilibrium ions in the sulphate electrolyte with the electrochemically active SO_3 gas is:

$$SO_3(g) + \frac{1}{2}O_2 + 2e^- \rightarrow SO_4^{2-} \tag{6.54}$$

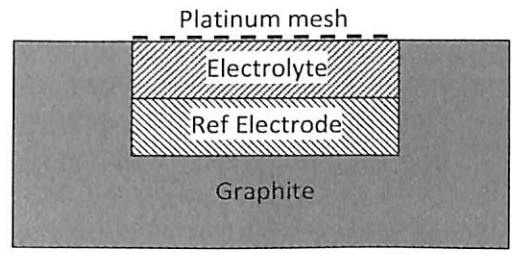

Figure 6.8 Cell assembly with isolation of reference electrode by embedding.

The half-cell reaction encountered at electrode-electrolyte is:

$$2Ag \rightarrow 2Ag^{\cdot} + 2e \tag{6.55}$$

Thus the complete redox reaction for the cell configuration,

$$Ag: Ag_2SO_4 / Electrolyte / Platinum \tag{6.56}$$

can be obtained by combining reactions;

$$2Ag + SO_3(g) + \frac{1}{2}O_2 \rightarrow Ag_2SO_4. \tag{6.57}$$

The inlet SO_2 concentration which is causing the above reaction can be calculated from the Nernst equation with knowledge of thermodynamic data for SO_2, SO_3 and Ag_2SO_4 and oxygen partiar pressure using Nernst equation.

Extending this analogy for gas sensors, with one reference gas (') electrode and another test gas (") electrode, one can arrive at SO_3 gas sensor as:

$$E = \frac{RT}{nF}\log\left(\frac{P''_{SO_3}\,P''_{O_2^{1/2}}}{P'_{SO_3}\,P'_{O_2^{1/2}}}\right) \tag{6.58}$$

With the novel idea of using metal/metal sulphate solid reference electrode, a lot of complexity in sensor fabrication has been removed making it convenient for field application, as the inconvenient reference gas electrode has been replaced by Ag/Ag_2SO_4 (metal/metal sulphate) reference electrode [9,10],

Reformatting the above Nernst equation for solid reference electrode,

$$E = E^0 + \frac{RT}{nF}\log\left(\frac{P''_{SO_3}\,P''_{O_2^{1/2}}}{a_{Ag_2SO_4}}\right) \tag{6.59}$$

here,

E^0 – emf due to free energy (Gibbs) of formation of Ag_2SO_4
R – is gas constant

P''_{SO_3} – partial pressure of SO_3gas

$P''_{O_2^{1/2}}$ – partial pressure of O_2 gas

αAg_2SO_4 – activity coefficient of Ag_2SO_4

$$E = \frac{-\Delta G^0(T)}{2F} + \frac{RT}{2F}\log\left(\frac{P''_{SO_3}\,P''_{O_2^{1/2}}}{a_{Ag_2SO_4}}\right) \tag{6.60}$$

Use of solid electrolytes in a galvanic electrochemical cell configuration has been of great interest in the detection of gaseous species; depending upon the characteristics, cell reaction delivers open circuit voltage (OCV). It can be calibrated and further used for manipulations for atomization of system. We shall deal with a particular case of SO_2 detection using SSEGS.

A typical experimental setup used for characterization of gas sensors using precomposed gas is shown in Figure 6.9. The known gas concentration and sensor OCV can be used for calibration.

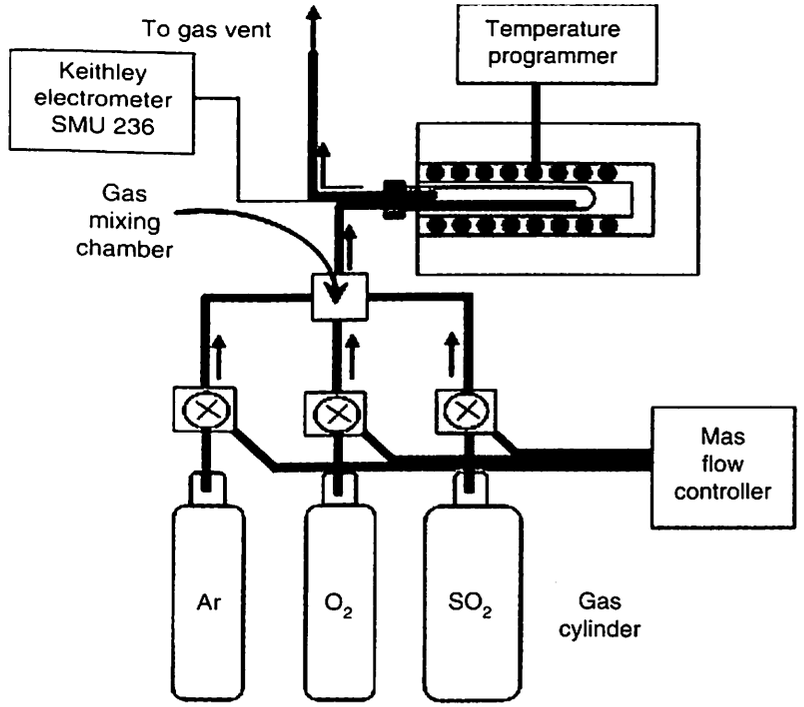

Figure 6.9 Schematic representation of the experimental setup for study of sensor characteristics.

The time dependence of emf toggling when SO_2 concentration switched from 50 to 1000 ppm at various temperatures has been depicted in Figure 6.10.

A sensor formed by utilizing $(96.37)Ag_2SO_4$:$(3.63)\ Y_2(SO_4)_3$ solid solution offers a good sensor option. Sensor emf toggling between 520 mV to 240 mV was observed for shuffling of SO_2 gas concentration from 50 ppm to 1000 ppm. A response time of 22 seconds is observed. The *prima-facie* sensor characterization indicates promising sensor behavior. A typical calibration curve can be shown in the Figure 6.10. A commercially available electrochemical gas sensor for oxygen is depicted in Figure 6.11. A typical calibration curve for

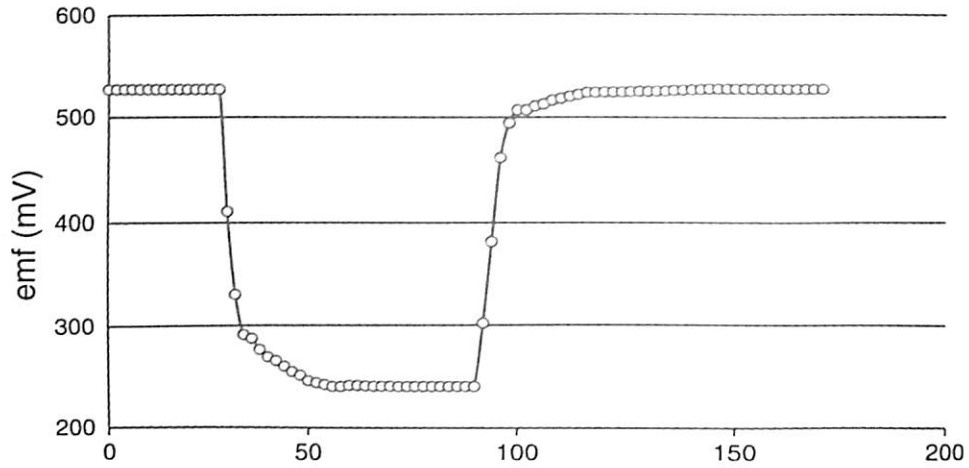

Figure 6.10 Variation of emf with time for swapping of SO_2 concentration from 50 to 1000 ppm.

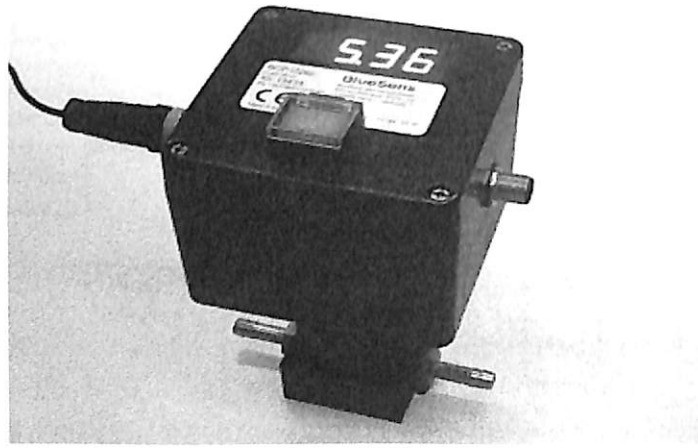

Figure 6.11 A typical commercially available electrochemical oxygen sensor.

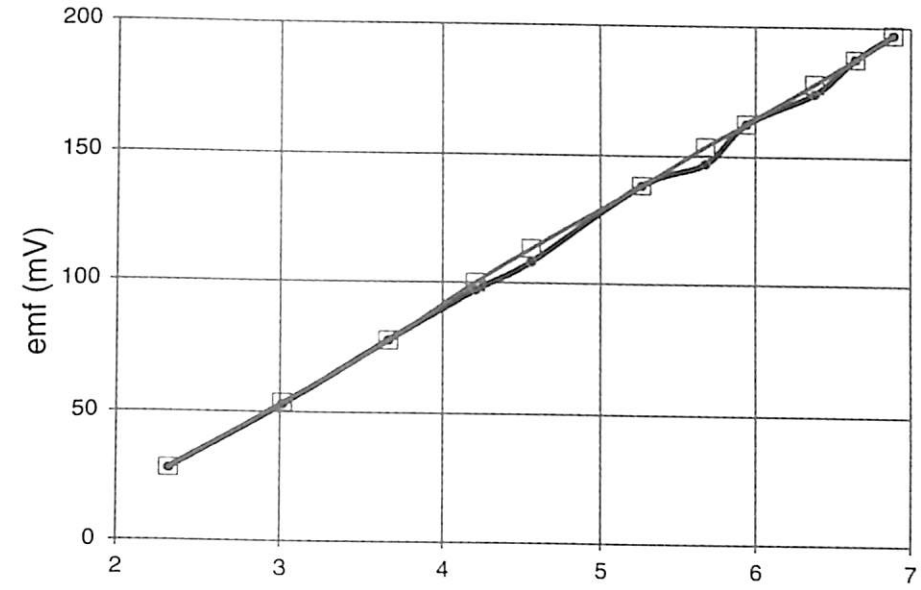

Figure 6.12 EMF as a function of SO_2 partial pressure at 558°C by Jacob & Jacob [60].

SO_2 sensor behavior observed by Jacob and Jacob [60] governed by Nernst equation is presented in Figure 6.12.

6.12 Conclusion

Solid electrolytes form a class of solids that offer ionic conductivity on par with liquid electrolytes. The solid form of the electrolytes offers fascinating advantages, which widens the application area. It also opens up a new domain for tailor-made suitable/desirable materials.

References

1. I. Tadao, *Solid State Ionics*, 2009 180.6 44. DOI: 10.1016/j.ssi.2008.10.021.
2. K.J. Lehovec, *Chem. Phy.* 1953 21(7) 1123 DOI:10.1063/1.1699148.
3. S. Chandra, *Super Ionic Conductors: Sensors and Applications*, North Holland, Amsterdam, 1981.
4. E. Madelung, *Phys. Zs.* 1918 XIX: 524–533.
5. R.D. Adams, M.D. Brice, F.A. Cotton, *Inorg. Chem.* 1974 13 (5), 1080 DOI: 10.1021/ic50135a014 1974.
6. J.M. Reau, J. Portier, *Solid Electrolytes*, P. Hagenmuller and W. Van Gool, Eds., Academic Press, Ch 9, 1978.

7. W.E. Danforth, J.H. Bodline, *J. Franklin Inst.* Vol. 260, p. 467, 1955.
8. R.W. West, N.M. Tallan, *J. Am. Ceramic Soc.* Vol. 48, p. 472, 1975.
9. T.A. Kuku, *Thin Solid Films* 325.1 246, 1998, DOI: 10.1016/S0040-6090(98)00430-1.
10. K.Singh, *Solid State Ionics* 199366, 5. DOI: 10.1016/0167-2738(93)90021-T.
11. E.N.S. Muccilloa, M. Kleitzb, *J. of Euro. Ceram. Society* 1996 16(4) 453, DOI:10.1016/0955-2219(95)00125-5.
12. L. Pandey, Om Prakash, R.K. Katare, D. Kumar, *Bull. Mater. Sci.* 1995 18(5) 563 DOI: 10.1007/BF02744842.
13. Q. Liu, W.L. Worrel, *Solid State Ionics* 1988 28-30(2) 1668. DOI: 10.1016/0167-2738(88)90439-0.
14. W. Weppner, *Solid State Ionics* 1981 3(4) 1. DOI:10.1016/0167-2738(81)90044-8 12.
15. W. Weppner, *Solid State Ionics* 1981 5 (3). DOI: 10.1016/0167-2738(81)90186-7 13.
16. W. Weppner, *Sens. and Actu.* 1987 12(2) 107. DOI: 10.1016/0250-6874(87)85010-2.
17. A. Tiwari, A.K. Mishra, H. Kobayashi, P.F. Turner, *Intelligent Nanomaterials*, Wiley-Scrivener Publishing LLC, USA, 2012 ISBN 978-04-709387-99, 2012 DOI: http://www.amazon.com/Intelligent-Nanomaterials-ebook/dp/B007DIAF16.
18. H. Kobayashi, *Adv. Mat. Lett.* 2012, 3(4), 265 DOI: 10.5185/amlett.2012.9001.
19. A. Tiwari, A.P. Mishra, S.R. Dhakate, R. Khan, S.K. Shukla, *Materials Letters* 2007 61(23–24) 4587 DOI:http://dx.doi.org/10.1016/j.matlet.2007.02.076
20. A. Tiwari, M. Prabaharan, R.R. Pandey, S. Li, *J. Inorg. Organomet. Polym. Mater.* 2010 20(2) 380 DOI: 10.1007/s10904-010-9354-9.
21. S.K. Barik, R.N.P. Choudhary, A.K. Singh, *Adv. Mat. Lett.* 2011 2(6) 419 DOI: 10.5185/amlett.2011.2228.
22. P.R. Das, B. Pati, B.C. Sutar, R.N.P. Choudhury, *Adv. Mat. Lett.* 2012, 3(1), 8-14 DOI: 10.5185/amlett.2011.4252
23. B.N. Parida, P.R. Das, R. Padhee, R.N.P. Choudhary, *Adv. Mat. Lett.* 2012, 3(3), 231 DOI: 10.5185/amlett.2012.2321
24. Rawat, M.; Yadav, K. L.; Kumar,A; Patel, P.K.; Adhlakha,N; Rani,J; Adv. Mat. Lett.2012, 3(4), 286 DOI: 10.5185/amlett.2012.2322
25. Singh, N. K.; Kumar, P; Rai, R; Kholkin, A L; Adv. Mat. Lett.2012, 3(4), 315 DOI: 10.5185/amlett.2011.9305
26. F.A. KroÈger, *The Chemistry of Imperfect Solids, 2nd Ed.*, 1974. DOI:http://www.worldcat.org/title/chemistry-of-imperfect-crystals-2-imperfection-chemistry-of-crystalline-solids/oclc/490295263
27. J. Maier, *Prog. Solid St. Chem.* 1995 23, 171. DOI:10.1016/0079-6786(95)00004-E

28. C.C. Liang, *J. Electrochem. Soc.* 1973 120, 1289. DOI: 10.1149/1.2403248
29. P. Padma Kumar, S. Yashonath, *J. Chem. Sci.* 2006 118(1) 135 DOI::10.1007/BF02708775
30. G.M. Torrie, J.P. Valleau, *J. Phys. Chem.* 1982, 86 (16), 3251. DOI: 10.1021/j100213a035
31. E.J.W. Verwey, J. Th. G. Overbeek, *Theory of the Stability of Lyophobic Colloids*, 1948, Elsevier, New York. DOI: 10.1002/pol.1949.120040321.
32. K. Lehovec, *J. Chem. Phys.*1953 21, 1123. DOI: 10.1063/1.1699148.
33. C.Wagner, *J.Phys.Chem.Solids* 197233, 1051. DOI:10.1016/S0022-3697(72)80265-8.
34. T. Jow, J.B. Wagner, *J. Electrochem. Soc.* 1979 126, 1963. DOI:10.1149/1.2128835.
35. J. Maier, *J. Phys. Chem. Solids* 1985 46, 309. DOI:10.1016/0022-3697(85)90172-6
36. J. Maier, *Nature Materials* 4, 805-815 (2005). DOI:10.1038/nmat1513.
37. R.C. Agrawal, R.K. Gupta, *J. Mater. Sci.* 1999 34, 1131. DOI: 10.1023/A:1004598902146.
38. M. Gauthier, A. Chamberland, *J. Electrochem. Soc.*1977 124, 1579. DOI:10.1149/1.2133114.
39. V. Ramaswamy, R.M. Vimalathithan, V. Ponnusamy, *Adv. Mat. Lett.* 2012, 3(1), 29-33 DOI: 10.5185/amlett.2011.4240.
40. H.Y. Liu, J.T. Hupp, M.J. Weave, *J. Electroanal. Chem. Interfacial Electrochem.* 1984 179, 1-2, 219. DOI: 10.1016/S0022-0728(84)80290-9.
41. S.H. Liu, C. Hinnen, C. Huong, N.R. Tacconi, K.M. Hoa, *J. Electroanal. Chem. Interfacial Electrochem.* 1984 176, 1–2, 325. DOI: doi:10.1016/S0022-0728(84)80327-7.
42. C.M. Mari, M. Beghi, S. Pizrini, *Sensors and Actuators B*, 1990, 2, 51-55. DOI: 10.1016/0925-4005(90)80008-N.
43. K. Singh, S.W. Anwane, S.S. Bhoga, *Solid State Ionics*, 1996 86-87, 187. DOI: 10.1016/0167-2738(96)00120-8
44. K. Singh, S.M. Pande, S.W. Anwane, S.S. Bhoga, *App. Phy. A*, 1998 66, 205. DOI: 10.1007/s003390050657
45. K. Singh, S.M. Pande, S.S. Bhoga, *Bull, Mater, Sci.* 1995 19(3) 237. DOI: http://www.ias.ac.in/jarch/bms/18/00000246.pdf.
46. S.W. Anwane, R.S. Anwane, *Adv. Mat. Lett.* 2012, 3(2), 77. DOI: 10.5185/amlett.2012.1314.
47. S.W. Anwane, *Adv. Mat. Lett.* 2012, 3(3), 204. DOI: 10.5185/amlett.2012.4332.
48. K. Singh, S.M. Pande, S.W. Anwane, S.S. Bhoga, *Bull. Electrochem.* 1996 12 (11-12) 625. DOI: 10.1007/BF02745557.
49. S.W. Anwane, *Adv. Mat. Lett.* 2013, 4(4) pp. 300-309. DOI:10.5185/amlett.2012.8404.
50. A. Atkinson, *Solid State Ionics* 1988 28±30, 1377. DOI:10.1016/0167-2738(88)90390-6.

51. B.J. Wuensch, H.L. Tuller, *J. Phys. Chem. Sol.* 1994 55, 975. DOI:10.1016/0022-3697(94)90117-1.
52. M. Aoki, Y.M. Chiang, I. Kosacki, J.R. Lee, H.L. Tuller, Y. Liu, *J. Am. Ceram. Soc.* 1996 79, 1169. DOI: 10.1111/j.1151-2916.1996.tb08569.x.
53. J.A.S. Ikeda, Y.M. Chiang, *J. Am. Ceram. Soc.* 1993 76, 2437 and 2447. DOI: 10.1111/j.1151-2916.1993.tb03964.x.
54. Chiang, Wang, Lee, *J. Microscopy* 2001 191-3,275. DOI: 10.1046/j.1365-2818.1998.00377.x.
55. V. Ramaswamy, R.M. Vimalathithan, V. Ponnusamy, *Adv. Mat. Lett.* 2012, 3(1), 29 DOI: 10.5185/amlett.2011.4240
56. C.M. Mari, M. Beghi, S. Pizrini, *Sensors and Actuators B*, 1990, 2, 51. DOI: 10.1016/0925-4005(90)80008-N.
57. P.H. Yang, J.H. Yang, C.S. Chen, D.K. Peng, G.Y. Meng, *Solid State Ionics* 1996 86-88, 1095.DOI: 10.1016/0167-2738(96)00275-5.
58. S. Suganuma, M. Watanabe, T.S. Kobayashi, Wakabayashi, *Solid State Ionics* 1999 126 (1-2) 175. DOI: 10.1016/S0167-2738(99)00220-9
59. K.T. Jacob, D.B. Jacob, *Electl. Soc.* 1989 126, 1824. DOI:bd84b405-7dae-4b25.../873630.pdf

7

Advanced Electronics: Looking beyond Silicon

Surender Duhan* and Vijay Tomer

Materials Research Lab, Department of Materials Science and Nanotechnology, Deenbandhu Chhotu Ram University of Science and Technology, Murthal, Sonepat (Hr), India

Abstract

The innovation and engineering of novel materials have always remained an underlying challenge for harnessing electronics technology. For over 50 years, silicon has ruled electronics technology, with progress inexorably following the prophetic statement from Gordon Moore, the co-founder of Intel, that the number of transistors on a silicon chip would grow exponentially with time, doubling every two years (Moore's law). Now the size limit of the building block of silicon technology is being approached, namely, transistor with its 22 nm limitation, raising the imminent question if Moore's law still holds good. This growth cannot be maintained forever, and so the search is on to find and use new materials which may be able to produce higher performance and better functionality, especially for electronics technology.

The authors of this chapter mainly focus on carbon-based electronics. Carbon-based materials offer a number of exciting possibilities for both new science and applications. Graphene possesses novel band structure, by which solids mimic the properties of relativisitic fermions and which offers the potential for high speed nanoscale electronics. Interesting properties have been investigated when sheets of graphene are rolled up to make carbon nanotubes, for example, both semiconducting and metallic nanotubes have been produced.

Keywords: Silicon, electronics, graphene, carbon nanotubes, CNT-FETs, transistors

**Corresponding author*: surender6561@yahoo.co.in

Ashutosh Tiwari and Sergiy Valyukh (eds.) Advanced Energy Materials, (295–326)
2014 © Scrivener Publishing LLC